DRAFT VERSION APRIL 11, 2023
Typeset using LaTeX **RNAAS** style in AASTeX631

# Stability analysis for general order central finite-difference hyperdiffusivity with time integrators of arbitrary accuracy

Wladimir Lyra[1]

[1]*New Mexico State University, Department of Astronomy, PO Box 30001 MSC 4500, Las Cruces, NM 88001, USA*

## ABSTRACT

Computational studies of astrophysical fluid dynamics often make use of explicit high-order artificial dissipation terms (i.e. hyperdiffusion and hyperviscosity), that behave as high-frequency filters, shortening the dissipation range while preserving numerical stability. In this contribution, I derive the Courant–Friedrichs–Lewy stability condition for general order hyperdiffusion, when discretized via central finite differences, to arbitrary order of accuracy in the Taylor expansion.

## INTRODUCTION

A hyperdiffusivity is a diffusivity operator that has a higher differential order than the regular Laplacian (Passot & Pouquet 1988; Shankar & Fogelson 2018). In one dimension, let $f$ be a signal, damped with a $b^{\rm th}$-order generalized diffusion according to the following evolution equation

$$\frac{\partial f}{\partial t} = D\frac{\partial^b f}{\partial x^b}, \tag{1}$$

where $D$ is a constant coefficient, $t$ is time, $x$ is a spatial coordinate, and $b = 2a$ with $a$ a positive integer. For $a = 1$, the system reduces to the usual diffusion equation, whereas $a > 1$ constitutes hyperdiffusion. Because it steepens the slope (in Fourier space) over which the system passes from high to low Reynolds numbers, hyperdiffusion is commonly used in numerical simulations of Navier-Stokes turbulence (Xu et al. 2023) to extend the inertial range while keeping the resolution affordable, albeit at the cost of an enhanced spurious accumulation of power near the beginning of the dissipative range (i.e. the bottleneck effect, Brandenburg & Sarson 2002; Frisch et al. 2008). In astrophysical fluid dynamics, hyperdiffusivity has been used in studies of gas in debris disks (Klahr & Lin 2005; Lyra & Lin 2013), planetary and exoplanetary atmospheres (Cho & Polvani 1996; Thrastarson & Cho 2011), the solar dynamo (Haugen & Brandenburg 2004; Pencil Code Collaboration et al. 2021), planet formation (Johansen et al. 2007; Lyra et al. 2008; Raettig et al. 2021) and satellite-disk interaction (Lyra et al. 2017). Popular choices for the parameter $a$ are $a = 2$ (Klahr & Lin 2005; Thrastarson & Cho 2011), and $a = 3$ (Haugen & Brandenburg 2004; Pencil Code Collaboration et al. 2021), though $a = 4$ or even $a = 8$ have been used (Cho & Polvani 1996; Lamorgese et al. 2005) .

The hyperdiffusion contribution to the Courant–Friedrichs–Lewy (CFL) condition takes a different Courant number than Laplacian diffusion. In most cases of physical importance, the hyperdiffusion will not dominate the timestep. Yet, it is important to derive the CFL condition in case it happens, so as to not underestimate the hyper-Courant number, leading to a lower timestep than necessary, adding numerical diffusion and increasing computational cost; or overestimate the hyper-Courant number, leading to exponential growth of grid-scale noise and numerical instability. Finally, this also has implications beyond Navier-Stokes, because hyperdiffusivity can be used to stabilize any advection-diffusion equation (e.g. Klahr & Lin 2005), by quenching noise beyond the scales the hyperdiffusivity operates.

In this contribution, I perform the von Neumann stability analysis of Eq. (1) when discretized with central finite difference, deriving the Courant condition that stabilizes this general hyperdiffusion. To the author's best knowledge, this is the first time that the general result (Eq. 14), the stability condition for hyperdiffusion of order $b$, discretized in $N$ spatial points centered-difference stencil, with a time integrator accurate to order $K$, is derived.

## SPATIAL DISCRETIZATION

Discretizing the signal with $N$ spatial points in the stencil, the central finite-difference $b$-th derivative evaluated at the point $i$ in a uniform grid is

$$\Delta^b f_i = \sum_{j=-M}^{M} c_j f_{i+j} \tag{2}$$

where $M \equiv (N-1)/2$, $N$ is assumed odd, and the coefficients $c$ of the numerical derivative are given by solving the system of $N$ equations

$$\sum_{j=-M}^{M} j^n c_j = b!\,\delta_{nb}, \tag{3}$$

for $0 < n < N-1$. Let $A$ be the amplitude of a Nyquist signal

$$f_i = A\, e^{-I\, k_{Ny} x_i} \tag{4}$$

where $k_{Ny} = \pi/\Delta x$ is the Nyquist wavenumber and $I$ is the imaginary number. Oscillating from $-A$ to $A$ with a $2\Delta x$ wavelength, the throughput of this signal when discretized with Eq. (2) is

$$\Delta^b f_i = -\kappa f_i, \tag{5}$$

where I define

$$\kappa \equiv \sum_{j=-M}^{M} |c_j|. \tag{6}$$

## TIME DISCRETIZATION

Having found the throughput, I consider now the time evolution of the Nyquist signal. For first-order timestepping

$$f_i^{(n+1)} = f_i^{(n)} + \Delta t \frac{\partial f_i^{(n)}}{\partial t}, \tag{7}$$

where the superscript $(n)$ refers to the quantity at time $t$, and $(n+1)$ to the quantity at time $t+\Delta t$. Substituting Eq. (1) and Eq. (5) into Eq. (7) leads to the following evolution for the amplitude after one timestep

$$A^{(n+1)} = A^{(n)}(1-\gamma), \tag{8}$$

where

$$\gamma \equiv \kappa C \tag{9}$$

is the spectral function and

$$C \equiv \frac{D\Delta t}{\Delta x^b}, \tag{10}$$

is the hyper-Courant number. The quantity in parentheses in Eq. (8) is the amplification factor, which leads to the stability condition for the first order timestepping

$$|1-\gamma| \leq 1. \tag{11}$$

## GENERALIZATION TO HIGHER-ORDER TIME DISCRETIZATION

The analysis above can be generalized for higher-order time integrators by considering a Taylor expansion to arbitrary order $K$

$$f_i^{(n+1)} = \sum_{k=0}^{K} \frac{\partial^k f_i^{(n)}}{\partial t^k} \frac{\Delta t^k}{k!} \tag{12}$$

Substituting Eq. (1) and Eq. (5) into Eq. (12) leads to

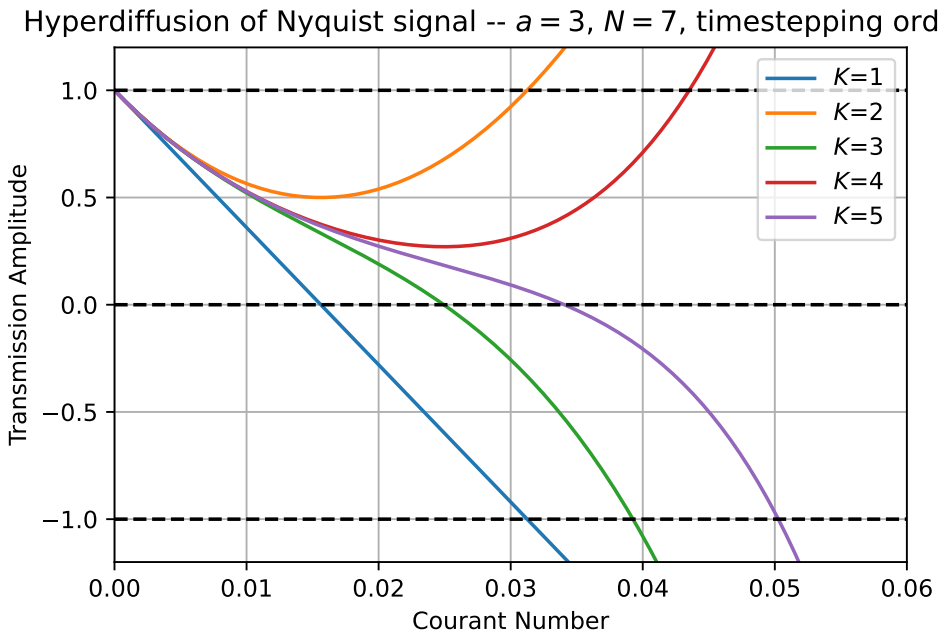


**Figure 1.** Transmission of the $a = 3$ (6th spatial derivative) of a Nyquist signal in a $N = 7$ points spatial stencil with a $K$-th order time integrator, as a function of Courant number.

$$A^{(n+1)} = A^{(n)} \sum_{k=0}^{K} (-1)^k \frac{\gamma^k}{k!}. \tag{13}$$

Again, the quantity in parentheses is the amplification factor. Thus, the general result for the stability condition is

$$\left| \sum_{k=0}^{K} (-1)^k \frac{\gamma^k}{k!} \right| < 1. \tag{14}$$

## APPLICATION

One can now choose the number of spatial points $N$ of the stencil, and the order $a$ of the hyperdiffusion to define the coefficients $c$ and their absolute sum $\kappa$. For $a = 3$ and $N = 7$, as in Pencil Code Collaboration et al. (2021), solving Eq. (3) yields $c = [1, -6, 15, -20, 15, -6, 1]$, so $\kappa = 64$.

I now choose the order $K$ of the time integrator. According to Eq. (14), this will generate a $K$-th order polynomial. I plot in Fig. 1 the polynomials up to $K = 5$. The roots correspond to zero transmission amplitude, or optimal cancelation of numerical noise. The values 1 and -1 correspond to marginal stability.

The polynomials also allow for analytical solutions. For a 3rd order integrator ($K = 3$),

$$A^{(n+1)} = A^{(n)} \left( 1 - \gamma + \frac{\gamma^2}{2!} - \frac{\gamma^3}{3!} \right) \tag{15}$$

This polynomial has one real root

$$\begin{aligned} \gamma &= 1 + \left(1+\sqrt{2}\right)^{1/3} - \left(1+\sqrt{2}\right)^{-1/3} \\ &\approx 1.6 \end{aligned} \tag{16}$$

or $C \approx 0.025$ if $\kappa = 64$. Marginal stability occurs at

$$\gamma = 1 + \left(4+\sqrt{17}\right)^{1/3} - \left(4+\sqrt{17}\right)^{-1/3} \approx 2.51 \tag{17}$$

or $C \approx 0.039$ again if $\kappa = 64$. For $K = 4$, i.e. the standard 4th order Runge-Kutta

$$A^{(n+1)} = A^{(n)} \left(1 - \gamma + \frac{\gamma^2}{2!} - \frac{\gamma^3}{3!} + \frac{\gamma^4}{4!}\right) \tag{18}$$

and marginal stability occurs at

$$\gamma = \frac{4}{3} + 2\left(\frac{43}{54} + \frac{\sqrt{29}}{6}\right)^{1/3} - \frac{10}{9}\left(\frac{43}{54} + \frac{\sqrt{29}}{6}\right)^{-1/3} \approx 2.79 \tag{19}$$

or $C \approx 0.044$ for the same choice of $\kappa$.

## REFERENCES


Brandenburg, A., & Sarson, G. 2002, Physics Review Letters, 88, 055003

Cho, J. Y. K., & Polvani, L. M. 1996, Physics of Fluids, 8, 1531

Frisch, U., Kurien, S., Pandit, R., Pauls, W., Ray, S. S., Wirth, A., & Zhu, J.-Z. 2008, Phys. Rev. Lett., 101, 144501

Haugen, N., & Brandenburg, A. 2004, Physical Review E, 70, 026405

Johansen, A., Oishi, J. S., Mac Low, M.-M., Klahr, H., Henning, T., & Youdin, A. 2007, Nature, 448, 1022

Klahr, H., & Lin, D. N. C. 2005, ApJ, 632, 1113

Lamorgese, A. G., Caughey, D. A., & Pope, S. B. 2005, Physics of Fluids, 17, 015106

Lyra, W., Johansen, A., Klahr, H., & Piskunov, N. 2008, A&A, 479, 883

Lyra, W., & Lin, M.-K. 2013, ApJ, 775, 17

Lyra, W., McNally, C. P., Heinemann, T., & Masset, F. 2017, AJ, 154, 146

Passot, T., & Pouquet, A. 1988, Journal of Computational Physics, 75, 300

Pencil Code Collaboration, Brandenburg, A., Johansen, A., Bourdin, P., Dobler, W., Lyra, W., Rheinhardt, M., Bingert, S., Haugen, N., Mee, A., Gent, F., Babkovskaia, N., Yang, C.-C., Heinemann, T., Dintrans, B., Mitra, D., Candelaresi, S., Warnecke, J., Käpylä, P., Schreiber, A., Chatterjee, P., Käpylä, M., Li, X.-Y., Krüger, J., Aarnes, J., Sarson, G., Oishi, J., Schober, J., Plasson, R., Sandin, C., Karchniwy, E., Rodrigues, L., Hubbard, A., Guerrero, G., Snodin, A., Losada, I., Pekkilä, J., & Qian, C. 2021, The Journal of Open Source Software, 6, 2807

Raettig, N., Lyra, W., & Klahr, H. 2021, ApJ, 913, 92

Shankar, V., & Fogelson, A. L. 2018, Journal of Computational Physics, 372, 616

Thrastarson, H. T., & Cho, J. Y.-K. 2011, ApJ, 729, 117

Xu, Y., Bingham, H. B., & Shao, Y. 2023, Applied Ocean Research, 134, 103535